An assessment of Sea Ice Extent Retrieval Based on HY-2A Scatterometer Data Using Other Satellite Products

Qimao Wang[1,2], Yingni Shi[3,4], Lijian Shi[1,2], Bin Zou[1,2]
[1]National Satellite Ocean Application Service, Beijing, China
[2]Key Laboratory of Space Ocean Remote Sensing and Application, State Oceanic Administration, Beijing, China
[3]Ocean University of China, Qingdao, China
[4]Mailbox NO 5111, Beijing, China
Email: qmwang@mail.nsoas.org.cn

KEY WORDS: Antarctica, Arctic, Sea ice extent, HY-2A, Scatterometer

ABSTRACT: A sea ice extent retrieval algorithm over the polar area based on scatterometer data of HY-2A satellite has been established. Four parameters are used for distinguishing between sea ice and ocean with Fisher's linear discriminant analysis method. The method is used to generate polar sea ice extent maps of the Arctic and Antarctic regions of the full 2013-2014 from the scatterometer aboard HY-2A (HY-2A-SCAT) backscatter data. The time series of the ice mapped imagery shows ice edge evolution and indicates a similar seasonal change trend with total ice area from DMSP-F17 Special Sensor Microwave Imager/Sounder (SSMIS) sea ice concentration data. For both hemispheres, the HY-2A-SCAT extent correlates very well with SSMIS 15% extent for the whole year period. Compared with Synthetic Aperture Radar (SAR) imagery, the HY-2A-SCAT ice extent shows good correlation with the Sentinel-1 SAR ice edge. Over some ice edge area, the difference is very evident because sea ice edges can be very dynamic and move several kilometers in a single day.

1. INTRODUCTION

Sea ice plays a key role in the Earth's climate system and its observation by satellite remote sensing sensors is an important task in climate research. Additionally, sea ice information is important for secure navigation and other offshore activities. Sea ice extent is one of parameters to describe the sea ice condition and microwave sensors are crucial tools because of their independence of sunlight and atmospheric influences capability.

Two types of microwave sensors are used to detect sea ice extent: passive microwave radiometers, which observe the natural emissions from ice surface, and active microwave scatterometers, which collect the energy reflected from ice surface. Since 1990s, C band Ku band microwave scatterometers, such as NSCAT, QuikSCAT and ASCAT, is used for detecting sea ice over polar area (Long and Drinkwater, 1994; Yueh et al., 1997). Remund/Long-NSCAT (RL-N) algorithm was demonstrated to map sea ice from Ku-band NSCAT data based on reconstructed backscatter images (Remund and Long, 1997a). An adaptation of RL sea ice extent algorithm for SeaWinds incorporates an iterative maximum likelihood discrimination method to statistically segment sea ice and ocean (Remund and Long, 2014). Maximum-likelihood (ML) discrimination is iteratively applied to segment ice and ocean populations statistically based on the multivariate microwave signatures. A sequence of binary processing operations and sea ice growth/retreat constraints using sea ice extent information from a previous day were used to filter residual noise caused by wind-roughend ocean surfaces or other microwave signature anomalies. Royal Netherlands Meteorological Institute (KNMI) developed a sea ice detection method for ERS, ASCAT and SeaWinds (Haan and Stoffelenm, 2001; Breivik et al., 2012), where computed residuals to geophysical ice and ocean model functions are interpreted as probabilities and then combined with prior information on the sea ice state using a Bayesian discrimination algorithm to produce sea ice maps. The main difference between the RL and KNMI sea ice detection algorithms is that the former ice and ocean cluster centroids in the 4-dimensional space of $\{\sigma_{\mathrm{H}}^0,\ \sigma_{\mathrm{V}}^0/\sigma_{\mathrm{H}}^0,\ \Delta\sigma_{\mathrm{H}@\mathrm{V}}^0\}$ combinations are replaced by actual geophysical model functions for ocean and ice in the original space of SeaWinds backscatter quadruplets $\{(\sigma_{\mathrm{H}}^0,\sigma_{\mathrm{H}}^0)_{\mathrm{fore}},\ (\sigma_{\mathrm{H}}^0,\sigma_{\mathrm{H}}^0)_{\mathrm{aft}}\}$(Belmonte et al., 2011). Abreu et al. (2002) showed that the retrieved ice edge successfully maps heavy areas of pack ice with ice concentrations above 70%, but it detects neither thin ice below 15-cm thickness nor areas of low ice concentrations. Other algorithms that combine the active polarization ratio (APR) of QuikScat L2B products and the SSM/I 19-GHz passive polarization ratio (PPR) have also been developed to detect new ice (Tonboe and Toudal, 2005).

HY-2A is the first Chinese satellite designed to monitor the dynamic marine environment. The purpose of this paper is to develop the sea ice extent over the polar area based on scatterometer data of HY-2A. In the following two sections, details of the used data and methods used are introduced. Assessments using other satellite data and other sea ice product are described in Section 4, and conclusions are drawn in Section 5.

2 Dataset

2.1 HY-2A scatterometer data

On August 16, 2011, the "HY-2A" satellite was launched in China. It is equipped with four remote microwave sensors: radar altimeter, microwave scatterometer, scanning microwave radiometer and calibration microwave radiometer. The satellite orbits the Earth at a flight height of 973 km and has an inclination angle of 99.34° and an orbit period of 104.46 minutes. The scatterometer aboard HY-2A satellite (hereafter referred to as HY2A-SCAT) employs a rotating pencil beam antenna which transmits and receives at 13.256GHz. Observations of backscatter cross section (σ^0) are collected in horizontally polarized (HH) inner beam and vertically polarized (VV) outer beam at incidence angles of 41° and 48°, respectively. The H-polarization covers a swath of 1350 Km and for V-polarization is 1700Km. HY2-SCAT share a similar sun-synchronous near polar with orbital inclinations of 99.34° at 971 Km, and running every day 13+11/14 circle. Hence, the coverage patterns of the sensors are enough that σ^0 measurements of HY2A-SCAT used for detecting polar sea ice.

To study conveniently polar sea ice, NSIDC (National Snow and Ice Data Center) specified a projection plane or grid tangent to Earth's surface at 70 degrees northern and southern latitude with little or no distortion in the marginal ice zone. The 25 km resolution grid dimensions was defined by 448×304 and 332×316 in Arctic and Antarctic, respectively. The HY2A-SCAT daily 13+11/14 track σ^0 measurements are reconstructed to a polar plane grid using polar stereographic projection formulae and the resolution is 25km as same as transform previous. Of course, each pixels on polar grid contain multiple different azimuth and incidence σ^0 measurements or none. Fig 1 exhibits the HY2-SCAT ability of observing polar zone, because Antarctic continent restricts sea ice to extend only to about 75 degrees south latitude, and Arctic sea ice extend all the way to the North Pole.

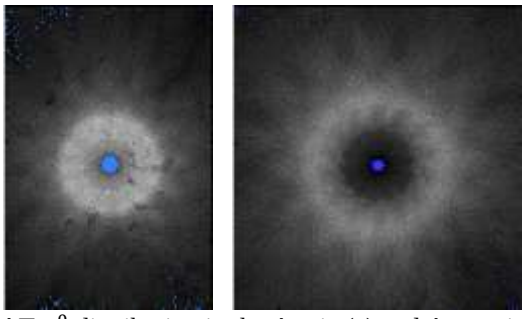

Fig. 1. Reconstructed HY2A-SCAT σ^0 distribution in the Arctic (a) and Antarctic (b) on September 20, 2013. The average daily north and south images have 0~40 σ^0 per pixel and major concentration in 5~25 and 3~15 observations, respectively. (The blue is no observation and other represents effective observation)

2.2 Sea ice concentration from NSIDC

National Snow and Ice Data Center (NSIDC) supplies sea ice concentrations (SIC) for both the Northern and Southern Hemispheres with NASA Team algorithm and brightness temperature data derived from the following sensors: the Nimbus-7 Scanning Multichannel Microwave Radiometer (SMMR), the Defense Meteorological Satellite Program (DMSP) -F8, -F11 and -F13 Special Sensor Microwave/Imagers (SSM/Is), and the DMSP-F17 Special Sensor Microwave Imager/Sounder (SSMIS). The data are provided in the polar stereographic projection at a grid cell size of 25 x 25 km (Cavalieri et al., 1996).

2.3 SAR imagery

Polar View, an international consortium providing a wide variety of earth observation products that monitor the Polar Regions and mid-latitude areas affected by ice and snow, provides a near-real-time sea ice information service for ship operators. Full resolution SAR imageries of Sentinel-1 and Radarsat-2 is supplied from Polar View's website with Geotiff format. With high spatial resolution, SAR imagery is used for ice edge validation in small localized regions in this study.

3 Method

Combined Fisher's linear discriminant analysis method and image erosion and dilation techniques, the sea ice extent is effectively mapped using four parameters of HY-2 scatterometer measurements. Figure 2 show the flowchart of the algorithm and each step is described in the following sub-sections.

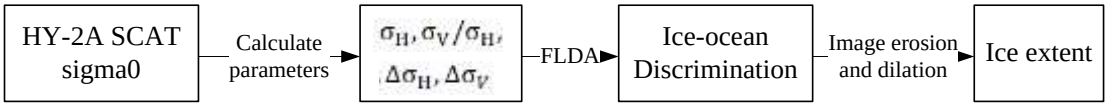

Fig. 2. Flowchart of algorithm

3.1 Parameter Calculation

In this study, four parameters are used for distinguishing between sea ice and ocean: mean HH backscatter (σ_H) per pixel at incidence of 41°; backscatter polarization Ratio (σ_V/σ_H) per pixel for VV and HH; daily standard deviation per pixel for HH ($\Delta\sigma_H$); daily standard deviation per pixel for VV ($\Delta\sigma_V$). Mean VV backscatter (σ_V) per pixel at incidence of 48° is not used because it has the same trend with σ_H. Fig. 3 shows this parameter images and the land mask is provided from NSIDC. Unfortunately, the VV or HH σ^o measurements per pixel in daily image probably not exist because of no observation, which result in σ_V/σ_H, $\Delta\sigma_{H,V}$ unavailable for coincident pixel. Therefore less than two HH and VV measurements are regarded as bad pixel not discriminating sea ice. To remedy that we loan the previous day category to replace today.

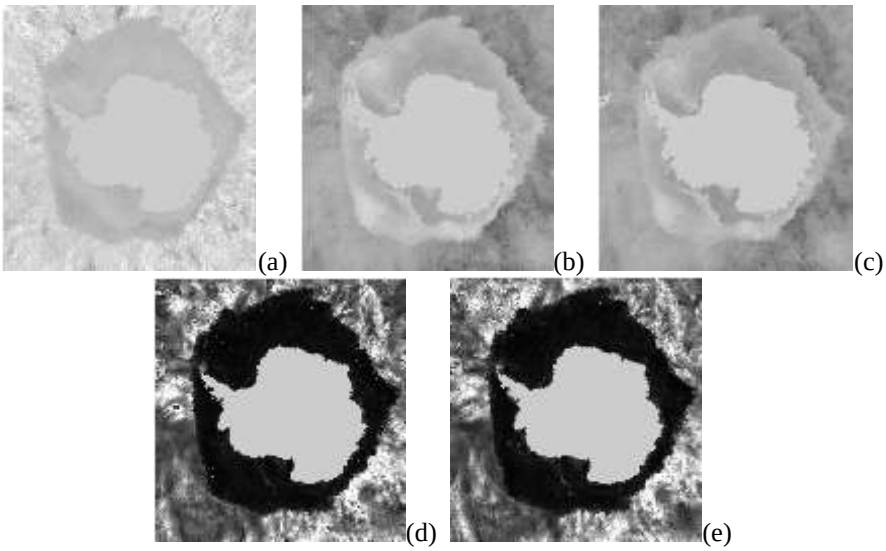

Fig. 3. Five parameter images are σ_V/σ_H (a), σ_H(b), σ_V(c), $\Delta\sigma_H$(d) and $\Delta\sigma_V$(e) on September 20, 2013. They contain 332×316 piexls with a space dimension of 25km in the Antarctic (Arctic images are not shown). Lighter greys without central continent indicate larger polarization distinctions in (a), higher σ^0 reception in (b) and (d), and higher σ^0 variability in (c) and (e).

In generally, polarization ratio (σ_V/σ_H) react to the backscatter difference of polarization and incidence angle rely on ocean and sea ice, in other words, because sea ice is strongly isotropic in incidence angle than ocean surfaces (Early and Long, 1997), the polarization ration (in decibels) is low in sea ice portions of the image and relatively higher in ocean areas (Remund and Long, 2014). Regrettably, high wind induces roughness on ocean surface, thus some ocean packs exhibit low polarization ratio close to sea ice (Remund and Long, 1999). In order to overcome this, the horizontally polarized mean measurements (σ_H) and daily standard deviation $\Delta\sigma_{H,V}$ are combined for ice-ocean classification. The h-pol mean measurements was chosen instead of the v-pol, because of it has much lower backscatter over ocean and sea ice has similar signatures. Meanwhile, daily standard deviation ($\Delta\sigma_{H,V}$) carries backscatter response depends on azimuthal and temporal, and sea ice backscatter signatures have been demonstrated that azimuthal dependences lower than ocean (Early and Long, 1997; Remund et al., 1997b).

3.2 Ice-ocean Discrimination

The ice-ocean discrimination achieved through Fisher's linear discriminant analysis (FLDA). This arithmetic fully utilizes the four priori feature parameters of ice-ocean and, by assuming multivariate normal distributions for the two classes, finds the optimal projection vector derived from Fisher's criterion peak for maximum infra-class margin and minimum inter-class cohesion in new small dimensional space. That is, the data belonging to the same category would be located near and the data belonging to the different categories would be located far. Of course, the FLDA is linear feature extraction classification method of supervised learning, and the feature parameter sample position of ice-ocean

from HY2A-SCAT is computed by all included ice flagged pixels in the NASA Team sea ice extent (provided by NSIDC).

Assuming that n sample with d dimensions are classified to two classes, and named $x_1, \ldots, x_n \in R^d$, n_1 in front of sample belong to class ω_1, the rest of n_2 belong to class ω_2, both obey Gaussian distribution with covariance matrix. Each kind of sample mean μ_i ($i = 1,2$) and the overall sample mean be

$$\mu_i = \frac{1}{n_i} \sum_{x \in \omega_i} x \quad i = 1,2 \qquad (1)$$

$$\mu = \frac{1}{n} \sum_{i=1}^{n} x_i \qquad (2)$$

The infra-class dispersion matrix S_b and the inter-class dispersion matrix S_w can be

$$S_b = \sum_{i=1}^{\omega} p(i)(\mu_i - \mu)(\mu_i - \mu)^T, \mathrm{p(i)} = \frac{n_i}{n} \qquad (3)$$

$$S_w = \sum_{i=1}^{\omega} \frac{p(i)}{n_i} \sum_{x \in \omega_i} (x - \mu_i)(x - \mu_i)^T, \quad i = 1,2 \ , \qquad (4)$$

respectively. To satisfy lower coupling of infra–class and higher polymerization of inter-class. Namely, the infra-class variance more important than the inter-class variance in the discrimination. Then, Fisher's criterion is introduced to seek a hyper plane φ to maximize $\frac{\varphi^T S_b \varphi}{\varphi^T S_w \varphi}$ and optimally separate two classes, and φ is explicitly given in the form

$$\varphi = S_w^{-1} S_b \qquad , (5)$$

by solving a general eigenvalue problem as the eigenvector corresponding to the largest eigenvalue of the matrix $S_w^{-1} S_b$. With this method, we can estimate the polar sea ice extent as Fig. 4a. While the ice edge can be syllabify observed, errors still exist, indicating that residual error filtering is required to improve the ice mapping.

3.3 Misclassification Reduction

Because the no observations and parameter controls, the parameters of some pixels in daily polar gird images cannot discriminate between sea ice and ocean. For processing the operational HY2A-SCAT daily sea ice extent, the NASA Team sea ice extent (archived by NSIDC) is initially as priori information to complement the unclassified pixels whatever sea ice or ocean, and mapping the first intact HY2A-SCAT sea ice extent in polar region. Later the previous day's sea ice extents of HY2-SCAT are regarded as background field for independently producing the real-time sea ice extent maps, such as Fig. 4b expression.

However, high persistent winds over the ocean can cause ocean pixels to be misclassified as ice, and other physical mechanisms may also cause sea ice to be misclassified as ocean. These misclassifications occur in patch or isolated pixels during the imaging period, and the former is much more common than the latter. Polar sea water connectedness contributes to the elimination of misclassified as ocean in the ice by using the image erosion and dilation techniques (Remund et al., 2000). This adopts a diamond structure element of radius 2 to implement primarily image erosion for eliminating small particles ocean noise and smoothing right ocean edge, and secondly image dilation for recovering ocean areas. Next, the misclassified as ice in the ocean is a certain distance from the main ice, relative to the previous day's maximum ice edge, all blocks of grow ice is identified by using the region growing techniques, and get a 100-km maximum edge change per day threshold, for eliminating over-growth ice that is misclassified as ice in the ocean. An example of the final sea ice extent is shown in Fig. 4c.

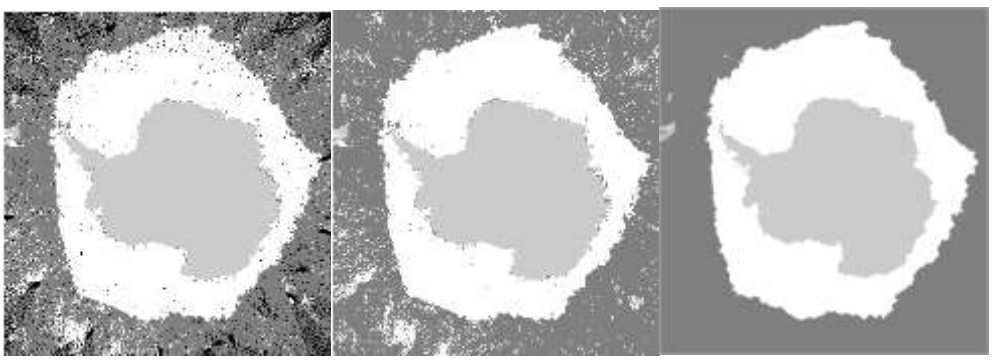

Fig. 4. These grayscate maps of Antartic sea ice on September 20, 2013 through this steps: (a) FLDA discrimination with the affection of no observations or invalid parameters(black portion); (b) no observations elimination depending on the preivous day's categories; (c) misclassification reduction by binary image processing methods.

4 Result

The algorithm described above section is used to generate polar sea ice extent maps of the Arctic and Antarctic regions for each day of 2013 from HY-2A-SCAT backscatter data. A time series of ice mapped imagery can be used in the removal of sea ice regions in scatterometer wind processing and ice edge evolution studies. In this section, the ice extent maps are compared to the sea ice concentration products and SAR imagery.

4.1 Sea Ice Mapping

As mentioned previously, the FLAD algorithm is imported to produce operational polar daily ice extent imagery in the HY2 satellite mission, which is classified by dynamic threshold based on predicated ice extent in winter (i.e. from this year's October to next year's June). Fig. 5 shows the seasonal and geographical sea ice products derived from HY2A-SCAT for a limited subset of days. For Arctic sea ice imagery, the image sequence of largest stage, retreat, trough period and growth is separated for exhibition. In addition, Antarctic images of low ebb, expansion, largest stage and melt parse similarly demonstrate the seasonal variation of ice pack.

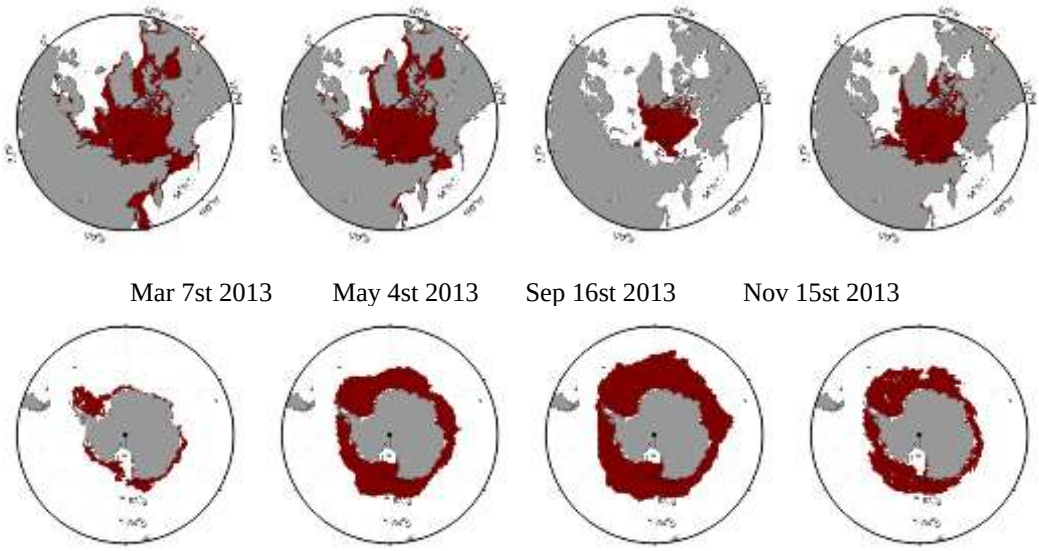

Fig. 5. Daily Polar sea ice extent and Arctic sea ice type from HY2-SCAT (except Sep 16st 2013, because it is beyond the scope of ice type determination)

4.2 Comparison with SSMIS sea ice concentration

Comparisons were made by comparing the ice extent results of the proposed method with SIC operational products of SSMIS. The two products have the same projection and spatial resolution. The total sea ice extent area is used as a parameter. This parameter of HY-2A-SCAT is calculated by summing the areas of all ice-masked pixels in its product. In order to compare datasets, SIC of SSMIS are threshold at various concentration levels (0%, 15% and 30%) to obtain multiple ice edges for comparison. The total ice areas results for the entire 2013 of different products are shown in Fig. 6a for the Arctic and Fig. 6b for the Antarctic. The products of HY-2A-SCAT during day 132-140 are missing because of the sensor's instability. The results show that the seasonal change of HY-2A-SCAT is similar with that of SSMIS. For both hemispheres, the HY-2A-SCAT extent correlates very well with SSMIS 15% extent for the whole year.

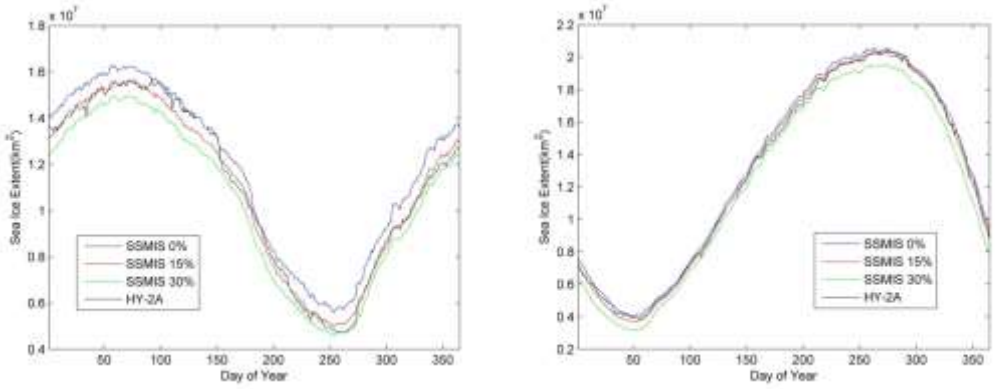

Fig. 6. Arctic (a) and Antarctic (b) daily total sea ice area of 2013. The HY-2A-SCAT and SSMIS 0%, 15%, and 30% ice extents are shown for comparison.

In order to illustrate the comparisons, σ_H image over Chukchi Sea of Oct. 23, 2015 is shown in Fig. 7. HY-2A-SCAT ice extent and 15% contour of SSMIS' SIC are overlapped with red and blue color, respectively. Over the bottom left part of Fig. 7, the HY-2A-SCAT's result matches the SSMIS' 15% contour very well. But over the center part of Fig. 7, the result of HY-2A-SCAT underestimates the sea ice extent and 15% contour of overlaps the ice edge of σ_H image obviously.

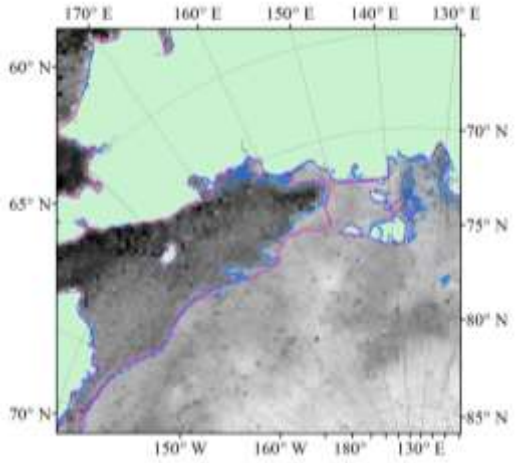

Fig. 7. Sea ice edge comparisons over Chukchi Sea of Oct. 23, 2015. The background is the σ_H image of HY-2A-SCAT. The SSMIS 15% contour and HY-2A-SCAT ice edge is plotted in blue and red, respectively.

4.2 With SAR

The ice extent maps are compared with SAR imagery for qualitative visual comparison. For this study, several Sentinel-1 images were downloaded from Polar View's website and overlapped with ice extent maps in ArcGIS. Some sample SAR images are shown in Fig. 8. Fig. 8a and 8b show winter SAR mosaic over Greenland Sea of Oct. 23, 2015 and Nov. 4, 2015. The HY-2A-SCAT ice extent shows good correlation with the SAR ice edge. During the winter, ice growth is expected and some area is covered by new ice (red block), which is not detected by HY-2A-SCAT. Off-ice winds happened with the above new ice formation. The ice was blown southward and new ice was formed by cold northerly winds over the area of red block. The HY-2A-SCAT ice edge underestimates the ice extent in Fig 8a, which should correspond to the movement of ice edge on Oct. 23, 2015. So comparison of HY-2A-SCAT result with SAR is not straight forward, but it is another way to get the temporal variability of the ice edge.

Fig. 8c and 8d show summer SAR image over Antarctic of Oct. 20, 2015 and Sept. 28, 2015. In Fig. 8c the good correlation between HY-2A-SCAT extent and SAR ice edge may be due to obvious different between ice and water and low wind speed over local area. But over the red block of Fig. 8d the difference are very evident because sea ice edges can be very dynamic and move several kilometers in a single day. The HY-2A-SCAT edges represent averages over the entire day and the SAR imagery is a "snap-shot" of the ice edge at a particular time of day.

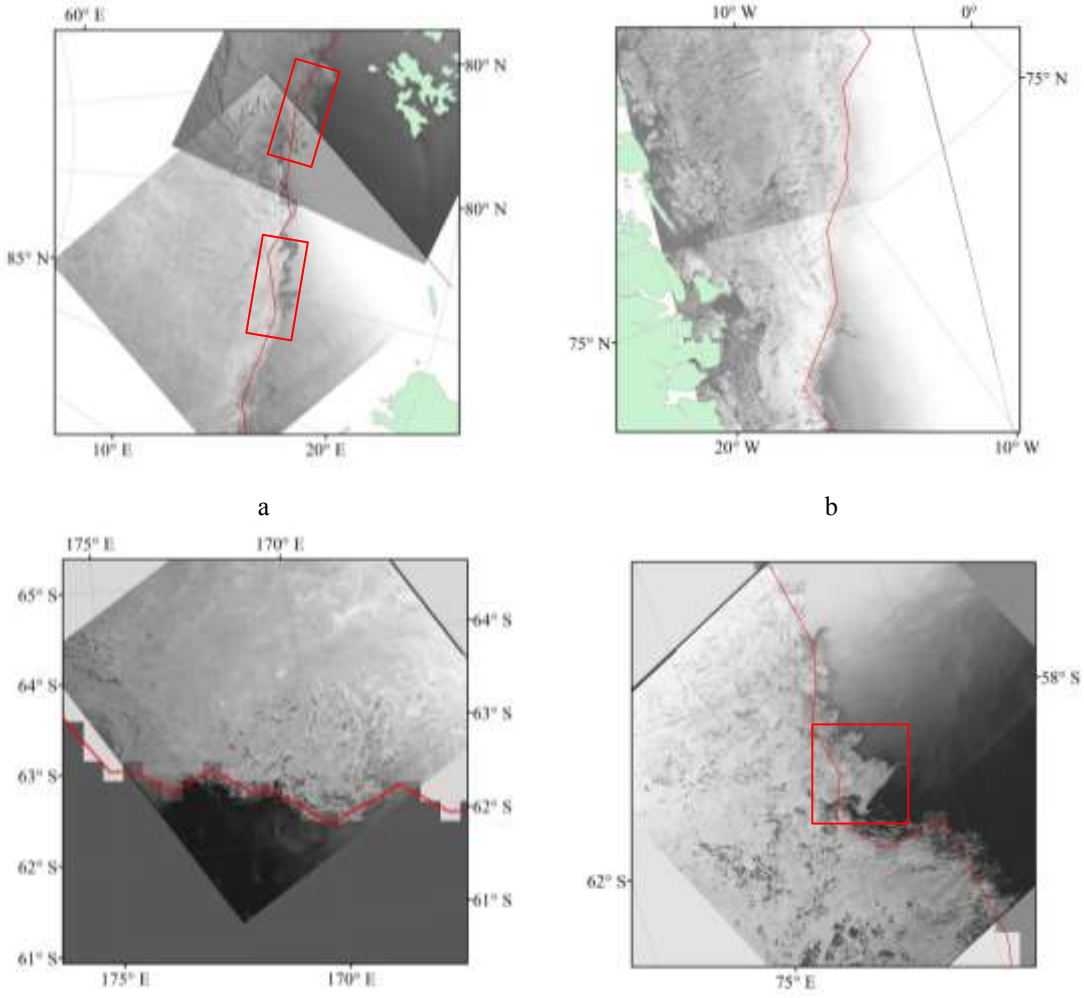

Fig. 8. Sentinel-1 imagery with HY-2A-SCAT ice extent. The image acquisition days are Oct. 23 (a), Nov. 4 (b), Oct. 20 (c), and Sept. 28 (d) of 2015.

5 Conclusion

This paper established an algorithm to map the sea ice extent over the polar area based on scatterometer data of HY-2A. The method is used to generate polar sea ice extent maps of the Arctic and Antarctic regions for each day of 2013 from HY-2A-SCAT backscatter data. The retrieved ice extent maps are assessed with the operational sea ice concentration products of SSMIS and SAR imagery. The main conclusion of this research can be stated as follows:

(1) Four parameters are used for distinguishing between sea ice and ocean: mean HH backscatter (σ_H), backscatter polarization Ratio (σ_V/σ_H), daily standard deviation per pixel for HH ($\Delta\sigma_H$), and daily standard deviation per pixel for VV ($\Delta\sigma_V$). Though Fisher's linear discriminant analysis method, these parameters are proven effective in identifying sea ice versus water. The image erosion and dilation technique is used to eliminate misclassified ice of open water.

(2) The time series of ice mapped imagery shows ice edge evolution and has the similar seasonal change trend with total ice area from SSMIS SIC data. For both hemispheres, the HY-2A-SCAT extent correlates very well with SSMIS 15% extent for the whole year.

(3) The ice extent maps are compared with SAR imagery for qualitative visual comparison. The HY-2A-SCAT ice extent shows good correlation with the Sentinel-1 SAR ice edge. The HY-2A-SCAT edges represent averages over the entire day and the SAR imagery is a "snap-shot" of the ice edge at a particular time of day. So over some ice edge area with high wind speed, the difference is very evident because sea ice edges can be very dynamic and move several kilometers in a single day.

Acknowledgement: We also thank the NSIDC for supplying the SIC data and the Polar View for supplying the SAR images. This work was supported by International Science and Technology Cooperation Project of China (contract No. 2011DFA22260), Open Research Fund of Key Laboratory of Digital Earth Science, Institute of Remote Sensing and Digital Earth, Chinese Academy of Sciences (contract No. 2014LDE009), the Chinese Polar Environment Comprehensive Investigation & Assessment Program by the State Oceanic Administration under contract No. 2015-02-04 and 2015-04-03-02.

References

Breivik, L., Eastwood, S., & Lavergne, T. (2012). Use of c-band scatterometer for sea ice edge identification. Geoscience & Remote Sensing IEEE Transactions on, 50, 2669-2677.

Cavalieri, D. J., C. L. Parkinson, P. Gloersen, and H. J. Zwally. 1996, updated yearly. Sea Ice Concentrations from Nimbus-7 SMMR and DMSP SSM/I-SSMIS Passive Microwave Data, Version 1. Boulder, Colorado USA. NASA National Snow and Ice Data Center Distributed Active Archive Center. http://dx.doi.org/10.5067/8GQ8LZQVL0VL.

De Abreu, R., Wilson, K., Arkett, M., & Langlois, D. (2002). Evaluating the use of QuikSCAT data for operational sea ice monitoring. Geoscience and Remote Sensing Symposium, 2002. IGARSS '02. 2002 IEEE International (Vol.5, pp.3032-3033 vol.5). IEEE.

Early, D. S., & Long, D. G. (1997). Azimuthal modulation of c-band scatterometer over southern ocean sea ice. IEEE Transactions on Geoscience & Remote Sensing, 35(5), 1201-1209.

Haan D. S., Stoffelen, A. (2001). Ice discrimination using ERS scatterometer, OSISAF Document KNMI-TEC-TN-120, EUMETSAT, http://www.knmi.nl/publications/.

Long, D. G., & Drinkwater, M. R. (1994). Greenland ice-sheet surface properties observed by the seasat-a scatterometer at enhanced resolution. Journal of Glaciology, 40(135), 213-230.

Remund, Q. P., & Long, D. G. (1997a). Automated Antarctic ice edge detection using NSCAT data. Geoscience and Remote Sensing, IGARSS '97. Remote Sensing - A Scientific Vision for Sustainable Development., 1997 IEEE International (Vol.4, pp.1841-1843 vol.4).

Remund, Q. P., Early, D. S., & Long, D. G., (1997b). Azimuthal modulation of Ku-band scatterometer σo over the Antarctic. MERS, Provo, UT, USA, Tech. Rep.97-02, 1997.

Remund, Q. P., & Long, D. G. (1999). Sea ice extent mapping using ku band scatterometer data. Journal of Geophysical Research Oceans,104(C5), 11515-11527.

Remund, Q. P., Long, D. G., & Drinkwater, M. R. (2000). An iterative approach to multisensor sea ice classification. IEEE Transactions on Geoscience & Remote Sensing, 38(4), 1843-1856.

Remund, Q. P., & Long, D. G. (2014). A decade of quikscat scatterometer sea ice extent data. IEEE Transactions on Geoscience & Remote Sensing, 52(7), 4281-4290.

Rivas, M. B., & Stoffelen, A. (2011). New bayesian algorithm for sea ice detection with quikscat. Geoscience & Remote Sensing IEEE Transactions on, 49(6), 1894 - 1901.

Tonboe, R., & Toudal, L. (2005). Classification of new-ice in the greenland sea using satellite ssm/i radiometer and seawinds scatterometer data and comparison with ice model. Remote Sensing of Environment, 97(3), 277–287.

Yueh, S. H., Kwok, R., Lou, S. H., & Tsai, W. Y. (1997). Sea ice identification using dual-polarized ku-band scatterometer data.Geoscience & Remote Sensing IEEE Transactions on, 35(3), 560-569.